C. T.-C. Nguyen, "Micromechanical filters for miniaturized low-power communications (invited)," to be published in *Proceedings of SPIE*: Smart Structures and Materials (Smart Electronics and MEMS), Newport Beach, California, March 1-5, 1999.

Micromechanical filters for miniaturized low-power communications

Clark T.-C. Nguyen

Center for Integrated Microsystems
Department of Electrical Engineering and Computer Science
University of Michigan
Ann Arbor, Michigan 48109-2122

ABSTRACT

With *Q*'s in the tens to hundreds of thousands, micromachined vibrating resonators are proposed as IC-compatible tanks for use in the highly selective filters of communications subsystems. To date, bandpass filters consisting of spring-coupled micromechanical resonators have been demonstrated in a frequency range from HF to VHF. In particular, two-resonator micromechanical bandpass filters have been demonstrated with frequencies up to 35 MHz, percent bandwidths on the order of 0.2%, and insertion losses less than 2 dB. In addition, free-free beam, single-pole resonators have recently been realized with frequencies up to 92 MHz and *Q*'s around 8,000. Evidence suggests that the ultimate frequency range of this high-*Q* tank technology depends upon material limitations, as well as design constraints—in particular, to the degree of electromechanical coupling achievable in micro-scale resonators.

Index Terms—resonators, microelectromechanical devices, micromachining, MEMS, micromechanical, bandpass, filter, fabrication, communications, transceiver, low power.

1. INTRODUCTION

Vibrating mechanical tank components, such as crystal and SAW resonators, are widely used for frequency selection in communication subsystems because of their high quality factor (*Q*'s in the tens of thousands) and exceptional stability against thermal variations and aging. In particular, the majority of heterodyning communication transceivers rely heavily upon the high *Q* of SAW and bulk acoustic mechanical resonators to achieve adequate frequency selection in their RF and IF filtering stages and to realize the required low phase noise and high stability in their local oscillators. At present, such mechanical resonator tanks are off-chip components, and so must interface with integrated electronics at the board level, often consuming a sizable portion of the total subsystem area. In this respect, these devices pose an important bottleneck against the ultimate miniaturization and portability of wireless transceivers. For this reason, many research efforts are focused upon strategies for either miniaturizing these components[1,2] or eliminating the need for them altogether.[3,4]

Recent demonstrations of micro-scale high-*Q* oscillators and mechanical bandpass filters with area dimensions on the order of 30 μm × 20 μm now bring the first of the above strategies closer to reality. Such devices utilize high-*Q*, on-chip, micromechanical (abbreviated "μmechanical") resonators[6] constructed in polycrystalline silicon using IC-compatible surface micromachining fabrication techniques, and featuring *Q*'s of over 80,000[7] under vacuum and center frequency temperature coefficients in the range of −10 ppm/^{o}C (several times less with nulling techniques).[8] To date, two-resonator micromechanical bandpass filters have been demonstrated with frequencies up to 35 MHz, percent bandwidths on the order of 0.2%, and insertion losses less than 2 dB.[9,11] Higher-order three-resonator filters with frequencies near 455 kHz have also been achieved, with equally impressive insertion losses for 0.09% bandwidths, and with more than 64 dB of passband rejection.[11] LF to MF (i.e., 20-300 kHz), high-*Q* oscillators, fully-integrated with sustaining CMOS electronics, have also been demonstrated in this technology.[7]

For use in many portable communications applications, however, higher frequencies must be achieved. Thus, frequency extension into the higher VHF and UHF ranges is presently the subject of ongoing research. This paper presents an overview of recent advances in frequency-selective MEMS devices aimed at both size reduction and performance enhancement of transceivers via miniaturization of high-*Q* signal processing elements. Specific results will be reported, including a review of recently demonstrated micromechanical resonators and filters in the VHF range, plus a brief mention of mixer+filter+gain stages based upon micromechanical technology. The remainder of this paper then focuses upon projections for the ultimate frequency range and performance of these communications devices.

Additional author information:
Full Address: 2406 EECS Bldg., 1301 Beal Ave, University of Michigan, Ann Arbor, MI 48109-2122
Tel: (734)764-1220, FAX: (734)763-9324, email: ctnguyen@eecs.umich.edu, http://www.eecs.umich.edu/~ctnguyen

2. ADVANTAGES OF MEMS IN COMMUNICATION TRANSCEIVERS

The front-end of a wireless transceiver typically contains a good number of off-chip, high-*Q* components that are potentially replaceable by micromechanical versions. Among the components targeted for replacement are RF filters, including image reject filters, with center frequencies ranging from 800 MHz to 2.5 GHz; IF filters, with center frequencies ranging from 455 kHz to 254 MHz; and high-*Q*, low phase noise local oscillators, with frequency requirements in the 10 MHz to 2.5 GHz range. As will be seen, it may soon also become possible to replace even the electronic mixers and active gain stages with micromechanical versions.[22] Figure 1 summarizes the major high-*Q* components potentially replaceable by micromechanical versions in a simplified super-heterodyne receiver architecture and illustrates the possibility for shrinking present-day board-level receiver implementations to single-chip ones via MEMS technology.

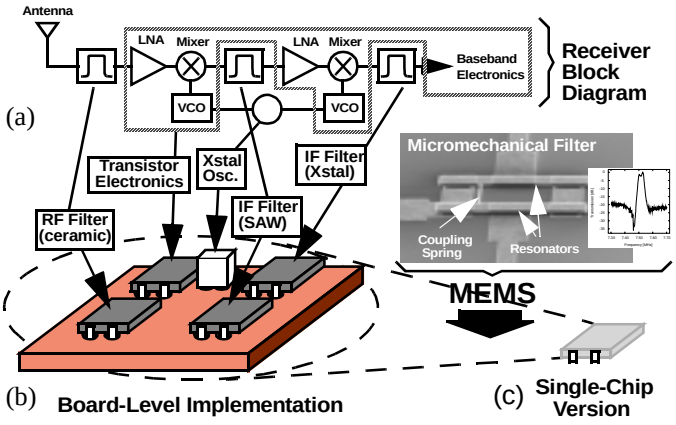

Fig. 1. (a) Simplified block diagram of a dual-conversion receiver. (b) Approximate physical implementation, emphasizing the board-level nature (many inductor and capacitor passives not shown). (c) Possible single-chip implementation using MEMS technology.

2.1. Miniaturization and IC-Compatibility

Reduced size constitutes the most obvious incentive for replacing SAWs and crystals by equivalent μmechanical devices. The substantial size difference between micromechanical resonators and their macroscopic counterparts is illustrated in Fig. 2, which compares a typical SAW resonator with a clamped-clamped beam micromechanical resonator of comparable frequency. The particular μresonator shown is excited electrostatically via parallel-plate capacitive transducers and designed to vibrate in a direction parallel to the substrate with a frequency determined by material properties, geometric dimensions, and stress in the material. Typical dimensions for a 100 MHz micromechanical resonator are $L \approx 12.9$ μm, $W=2$ μm, and $h=2$ μm. With electrodes and anchors, this device occupies an area of 420 μm^2 = 0.00042 mm^2. Compared with the several mm^2 required for a typical VHF range SAW resonator, this represents several orders of magnitude in size reduction.

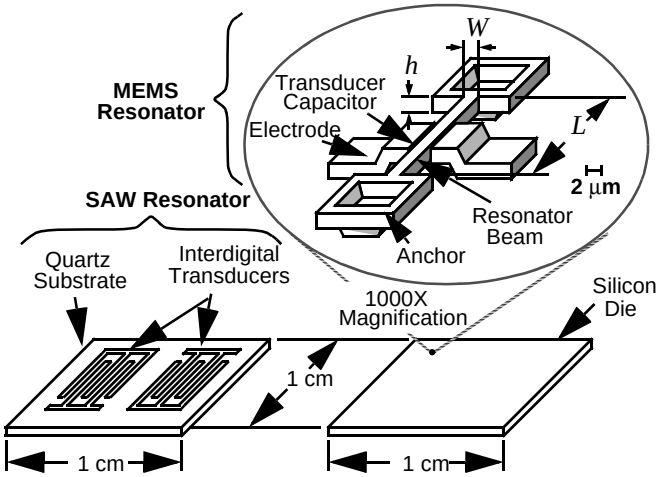

Fig. 2. Size comparison between present-day SAW resonator technology and the described high-*Q* μmechanical resonator technology.

A related incentive for the use of micromechanics is integrability. Micromechanical structures can be fabricated using the same planar process technologies used to manufacture integrated circuits. Several technologies demonstrating the merging of CMOS with surface micromachining have emerged in recent years,[12-14] and one of these is now used for high volume production of commercial accelerometers.[12] Using similar technologies, complete systems containing integrated micromechanical filters and oscillator tanks, as well as amplification and frequency translation electronics, all on a single chip, are possible. This in turn makes possible high-performance, single-chip transceivers, with super-heterodyne architectures and all the communication link advantages associated with them. Other advantages inherent with integration are also obtained, such as elimination of board-level parasitics that could otherwise limit filter rejections and distort their passbands.

2.2. Power Savings Via MEMS

Although certainly a significant advancement, miniaturization of transceivers only touches the surface of the true potential of this technology. MEMS technology may in fact make its most important impact not at the component level, but at the system level, by offering alternative transceiver architectures that emphasize selectivity over complexity to substantially reduce power consumption and enhance performance.

The power savings advantages afforded by MEMS is perhaps best illustrated by comparison with recent attempts to reduce the cost and size of wireless transceivers via increased circuit complexity. Specifically, in these approaches higher levels of

transistor integration and alternative architectures are used to reduce the need for the off-chip, high-*Q* passives used in present-day super-heterodyne transceivers, with obvious size advantages. Unfortunately, removal of off-chip passives often comes at the cost of increased power consumption in circuits preceding and including the analog-to-digital converter (ADC), which now must have higher dynamic ranges to avoid desensitization caused by larger adjacent channel interferers. A selectivity (or *Q*) versus power trade-off is clearly seen here.

To better convey this point, specific phenomena that give rise to receiver desensitization are illustrated in the diagram of Fig. 3(a), which depicts the signal flow for a desired signal at ω_{inf} with two adjacent interferers ($\Delta\omega$ and $2\Delta\omega$ away) from antenna to baseband in a conventional receiver architecture using *wideband* RF filters. As shown, due to nonlinearity in the low-noise amplifier (LNA) and phase noise in the local oscillator, the presence of interferers can potentially desensitize the receiver by (1) generating third-order intermodulation (IM_3) distortion components over the desired signal at the output of the LNA; and (2) aliasing superposed phase noise sidebands from the local oscillator onto the desired signal immediately after the mixer stage. In order to avoid such desensitization, the LNA must satisfy a strict linearity requirement, and the local oscillator a strict phase noise requirement, both of which demand significantly higher power consumption in these components. Similar increases in power consumption are also often necessary to maintain adequate dynamic range in subsequent stages (e.g., the A/D converter).

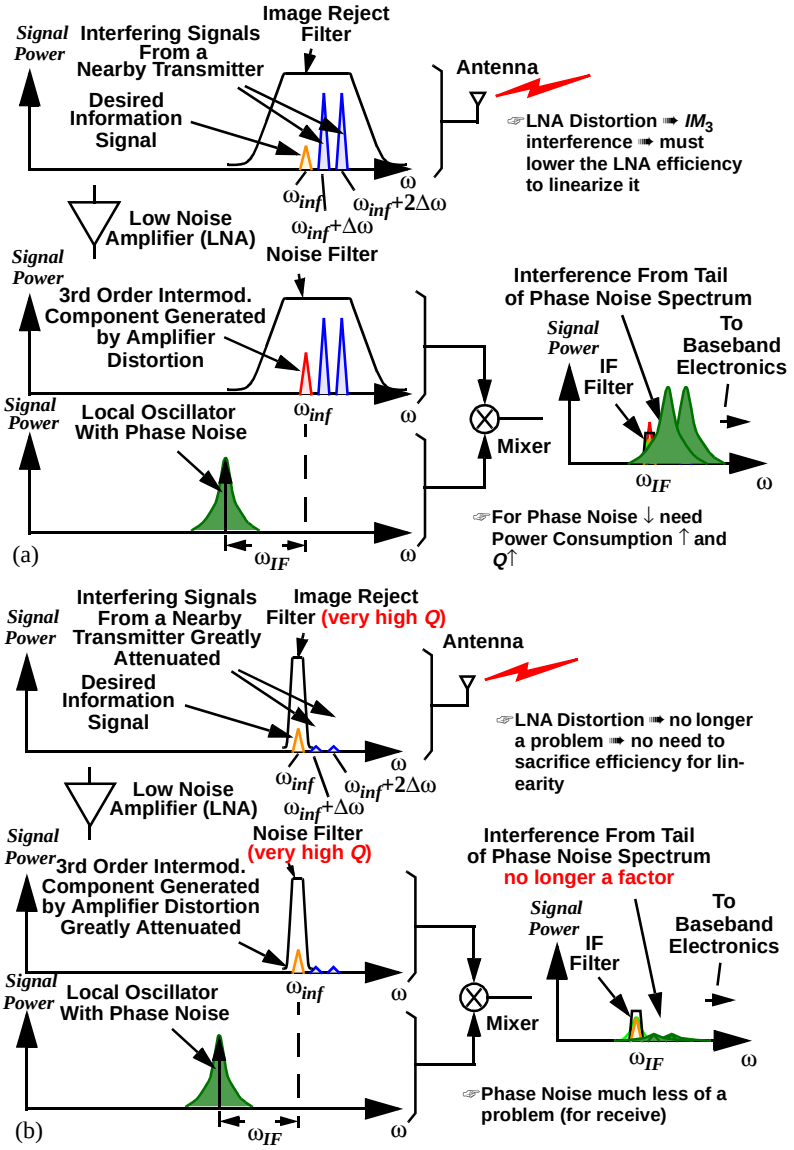

Fig. 3. Modified signal flow diagrams for (a) a conventional receiver using wideband RF filters; and (b) an RF channel-select receiver.

A method for eliminating such a waste of power becomes apparent upon the recognition that the above desensitization phenomena arise in conventional architectures only because such architectures allow interfering signals to pass through the RF filter and reach the LNA and mixer. If these signals were instead eliminated at the outset by a much more selective RF filter, then interference from IM_3 components and from phase noise sidebands would be greatly alleviated, as shown in Fig. 3(b), and specifications on linearity and phase noise could be greatly relaxed. The power savings afforded by such relaxations in specifications is potentially enormous, especially when considering the possibility of replacing conventional Class A or AB type amplifiers with more efficient topologies, such as Class E. The above discussion pertains to the receive path, but if channel-select filters with both sufficiently high *Q* and power handling capability are available and placed right before the transmitting antenna, similar power savings are possible for the *transmit* local oscillator and power amplifier, as well.

An architecture such as shown in Fig. 3(b) requires a tunable, highly selective (i.e., high-*Q*) filter capable of operation at RF frequencies. Unfortunately, partially due to their own high stability, high-*Q* filters are generally very difficult to tune over large frequency ranges, and MEMS-based filters are no exception to this. Although μmechanical resonators can be tuned over larger frequency ranges than other high-*Q* tank technologies, with voltage-controllable tuning ranges of up to 5% depending on design, a single micromechanical filter still lacks the tuning range needed for some wide-band applications

Thanks to the tiny size of micromechanical filters, however, there no longer needs to be only one filter. One of the major advantages of micromechanical filters is that, because of their tiny size and zero dc power dissipation, many of them (perhaps hundreds or thousands) can be fabricated onto a smaller area than occupied by a single one of today's macroscopic filters. Thus, rather than use a single tunable filter to select one of several channels over a large frequency range, a massively parallel bank of switchable micromechanical filters can be utilized, in which desired frequency bands can be switched in, as needed. The simplified block diagram for such a front-end architecture is illustrated in Fig. 4, where each filter switch combination corresponds to a single micromechanical filter, with input and output switches activated by the mere application or removal of dc-bias voltages (V_P, in later discussions) from the resonator elements. By further exploiting the switching flexibility of such a system, some very resilient frequency-hopping spread spectrum transceiver architectures can be envisioned that take advantage of simultaneous switching of high-Q micromechanical filters and oscillators.

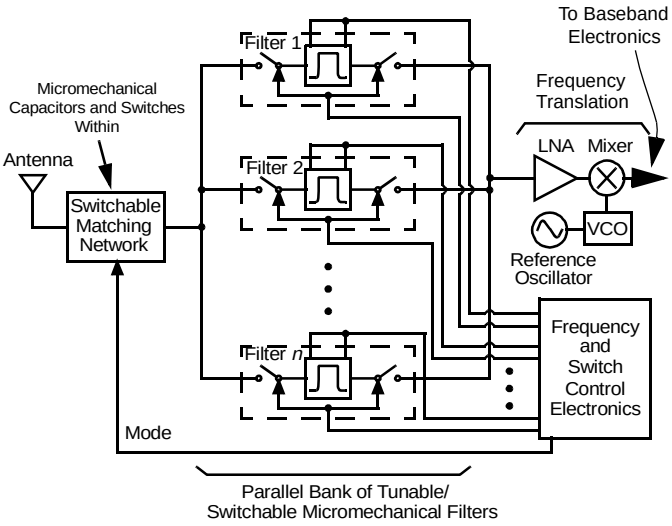

Fig. 4. Possible front-end receiver architecture utilizing a parallel bank of tunable/switchable micromechanical filters for a first stage of channel selection. Note that several micromechanical resonator devices can also be used within the frequency translation blocks as well.

In effect, frequency-selective devices based on MEMS technologies can potentially enable substantial power savings by making possible paradigm-shifting transceiver architectures that, rather than eliminate high-Q passive components, attempt to maximize their role with the intention of harnessing the Q versus power trade-off often seen in transceiver design. The next sections now focus upon the subject micromechanical resonator devices.

3. HIGH FREQUENCY MICROMECHANICAL RESONATORS

Micromechanical resonators comprise the fundamental building blocks for more complex frequency-selective functions, such as bandpass filters or tunable reference/voltage-controlled oscillators. As will be seen, such resonators and their specific interconnections dictate both the center frequency and bandwidth of a given micromechanical filter. Needless to say, careful mechanical resonator design is imperative for successful filter implementation. The selected μresonator design must not only be able to achieve the needed frequency, but must also do so with adequate linearity and tunability, and with sufficient Q.

For many sensor applications, such as accelerometers[15] or gyroscopes,[16] the lower the resonance frequency of the mechanical structure, the better the sensitivity of the device. Thus, the majority of previous micromachined mechanical devices aimed at sensor applications have been designed to resonate at very low frequencies, below 100 kHz. Designs with long spring lengths and large masses are common for these applications, and techniques that extend linearity and displacement amplitude, such as interdigitated comb-capacitive transducers and folded-beam suspensions,[6] are often used.

Such designs, however, are impractical for applications in the HF range, and beyond. In order to maximize resonance frequency, governed by the general expression

$$f_o = \frac{1}{2\pi}\sqrt{\frac{k_r}{m_r}}, \qquad (1)$$

the effective resonator spring stiffness k_r must be maximized, while its effective mass m_r minimized. The optimum HF or higher μresonator design should thus avoid the increased mass of a comb structure and the stiffness reduction of a folded-flexure.[6] For this reason, this work utilizes the simple clamped-

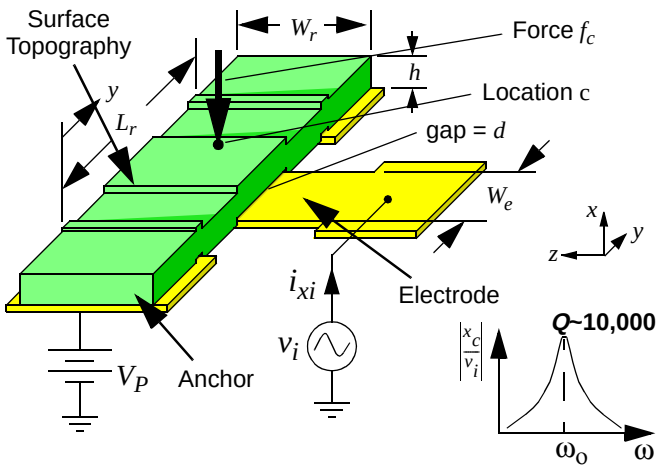

Fig. 5. Perspective view schematic of a clamped-clamped beam μmechanical resonator under a typical bias and excitation configuration. Note the mechanical input force f_c.

clamped beam resonator shown in Fig. 5 under a typical bias and excitation configuration.

The resonance frequency of this clamped-clamped beam depends upon many factors, including geometry, structural material properties, stress, the magnitude of the applied dc-bias voltage V_P, and surface topography. Accounting for these while neglecting finite width effects, an expression for resonance frequency can be written

$$f_o = 1.03\kappa\sqrt{\frac{E}{\rho}}\frac{h}{L_r^2}\left(1 - \left\langle\frac{k_e}{k_m}\right\rangle\right)^{1/2}, \text{ where } \left\langle\frac{k_e}{k_m}\right\rangle = \int_{0.5(L_r - W_e)}^{0.5(L_r + W_e)} \frac{V_P^2 \varepsilon_o W_r dy'}{k_m(y')(d(y'))^3}, \quad (2)$$

and where E and ρ are the Young's modulus and density of the structural material, respectively; ε_o is the permittivity in vacuum; h and L_r are specified in Fig. 5; the function $\langle k_e/k_m \rangle$ models the effect of an electrical spring stiffness k_e that arises when a bias voltage is applied across the electrode-to-resonator gap, and that subtracts from the mechanical stiffness $k_m(y)$; $d(y)$ is the electrode-to-resonator gap spacing as a function of location, which changes due to beam bending under a static V_P load; and κ is a scaling factor that models the effects of surface topography. For the μresonators of this work, κ is dominated by anchor step-up and finite elasticity effects,[17] which are predictable using finite element analysis (FEA).

3.1. Electromechanical Operation

To simplify future integration with transistor circuits, the μmechanical structures in this work are excited electrostatically via capacitive transducers. For the described clamped-clamped beam vertically resonant design, the transducer capacitor is formed between the resonator beam and an underlying electrode, shown in Fig. 5. Under normal operation, an input voltage, comprised of a dc-bias potential V_P and an ac signal v_i, is applied across the electrode-to-resonator transducer capacitor. This combination of voltages generates an electrostatic force between the electrode and resonator with the most dominant component at the frequency of v_i given by [6]

$$f_d = V_P \frac{\partial C}{\partial x} v_i, \quad (3)$$

where $\partial C/\partial x$ is the change in electrode-to-resonator capacitance per unit displacement of the resonator. When the frequency of v_i matches the resonance frequency, the beam begins to vibrate with a zero-to-peak displacement amplitude at the center of the beam given to first order (neglecting distributed stiffness over the electrode width) by

$$x_e = \frac{Qf_d}{k_{re}} = \frac{Q}{k_{re}} V_P \frac{\partial C}{\partial x} v_i, \quad (4)$$

creating a current i_x across the dc-biased time-varying electrode-to-resonator capacitor approximately given by

$$i_x = V_P \frac{\partial C}{\partial x}\frac{\partial x_e}{\partial t}, \quad (5)$$

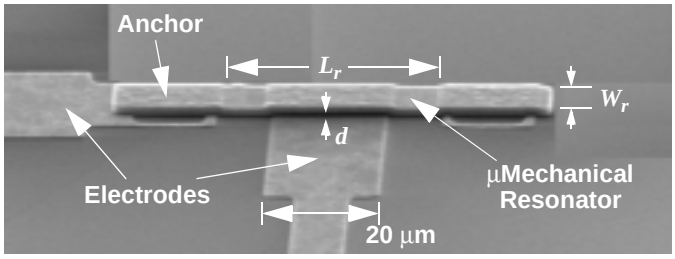

Fig. 6. SEM of an 8.5MHz clamped-clamped beam μmechanical resonator.

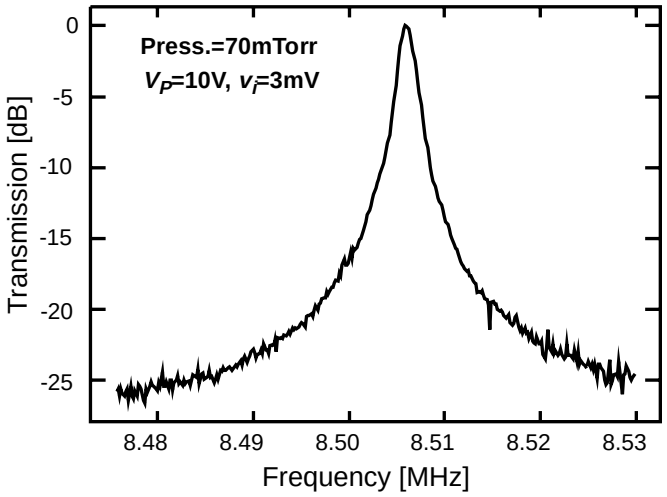

Fig. 7. Frequency characteristic for the micromechanical resonator of Fig. 6 measured with V_P=10V and v_i=3mV under 70mTorr vacuum.

where k_{re} is the stiffness at the electrode location (i.e., at the center of the beam), and $\partial C/\partial x$ is the change in electrode-to-resonator capacitance per unit displacement. When plotted versus input frequency, i_x traces out the bandpass biquad spectrum shown in Fig. 5. For the 8.5 MHz resonator of Fig. 7, a typical vibration amplitude is 170Å for a dc-bias of V_P=10V and an ac input voltage of v_i=3mV. Vibration amplitudes decrease as frequencies go up, since stiffness k_{re} rises with frequency. Note from (3) and (5) that with V_P=0V, no force or output current is possible (to first order), effectively making this device on/off switchable by the mere application or removal of V_P.

Figure 6 presents the scanning electron micrograph (SEM) of a surface-micromachined, clamped-clamped beam, 8.5 MHz μmechanical resonator. The frequency characteristic for this μmechanical resonator, measured under 70 mTorr pressure and linear drive conditions is presented in Fig. 7. The quality factor Q extracted from this plot is 8,000, which is plenty adequate for demonstration of low insertion loss filters. Note, however, that this Q is only achievable under vacuum, where viscous gas

damping is minimized.[18] Much lower *Q*'s on the order of hundreds are seen under atmospheric pressure.

3.2. Fabrication of Micromechanical Resonators

Due to a wide flexibility in geometry and electrode placement, plus an amenability to combination with integrated circuits, polysilicon surface micromachining[14] has so far been the preferred technology for fabricating high-*Q* μmechanical resonators, such as shown in Fig. 6. In this process, a series of film depositions and lithographic patterning steps—identical to similar steps used in planar IC fabrication technologies—are utilized to first achieve the cross-section shown in Fig. 8(a). Here, a sacrificial oxide layer supports the structural polysilicon material during deposition, patterning, and subsequent annealing. In the final step of the process, the wafer containing cross-sections similar to Fig. 8(a) is dipped into a solution of hydrofluoric acid, which etches away the sacrificial oxide layer without significantly attacking the polysilicon structural material. This leaves the free-standing structure shown in Fig. 8(b), capable of movement in three dimensions, if necessary.

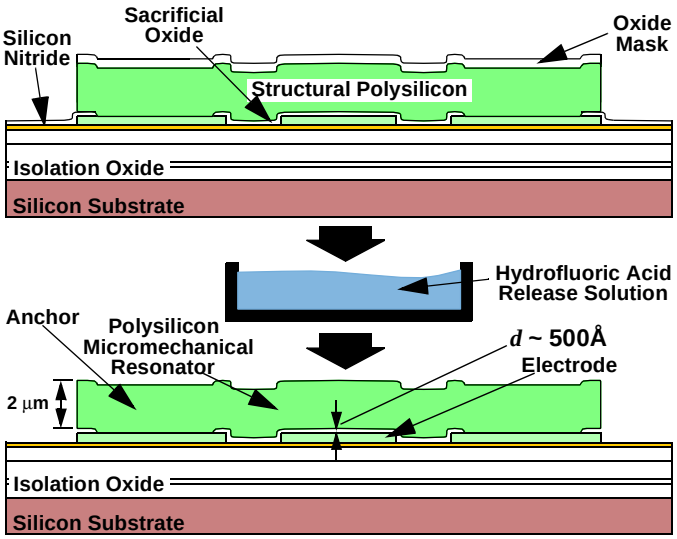

Fig. 8. Cross-sections depicting the fabrication sequence used to achieve micromechanical resonators. (a) Required film layers up to the release etch step. (b) Resulting free-standing beam following a release etch in hydrofluoric acid.

Because high stiffness is required to achieve HF or higher frequencies, the sticking yield loss mechanism so often seen with applications requiring more compliant suspensions (e.g., accelerometers[15]) is no longer a problem for resonator-based communication applications. Unfortunately, however, other yield loss mechanisms arise to replace stiction. In particular, as will be seen, very small electrode-to-resonator gaps (e.g., less than 500Å) will be required to achieve sufficiently small port impedances for filters based on micromechanical resonators. For instances where sub-500Å gaps are required, the ability to clear out etch residues from gaps during release etching becomes of major importance, and the surfactant-enriched hydrofluoric acid solutions often used for ULSI processing take on an enhanced significance.

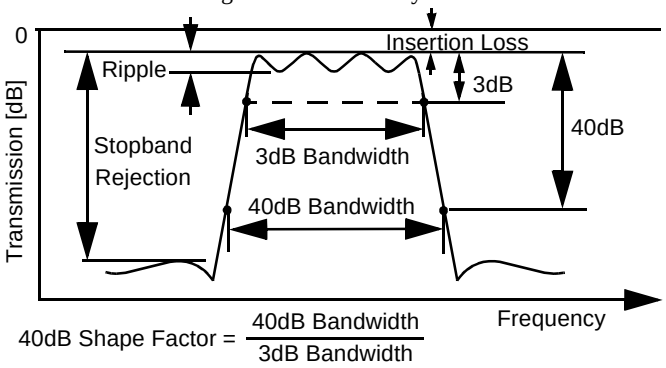

Fig. 9. Parameters typically used for filter specification.

4. MICROMECHANICAL FILTERS

The measured spectrum of Fig. 7 represents the frequency characteristic for a second-order, single-pole, bandpass filter centered at 8.5 MHz. Although useful for some applications, such as pilot tone filtering in mobile phones, second-order filter characteristics are generally inadequate for the majority of communications applications. Rather, bandpass filters such as depicted generically in Fig. 10 are required, with flatter passbands, sharper roll-offs, and greater stopband rejections.

4.1. General Mechanical Filter Design Concepts.

To achieve the characteristic of Fig. 9, a number of micromechanical resonators are coupled together by soft coupling springs,[9,10,19] as illustrated schematically in Fig. 10(a) using ideal mass-spring-damper elements. By linking resonators together using (ideally) massless springs, a coupled resonator system is achieved that now exhibits several modes of vibration. As illustrated in Fig. 11 for the coupled three-resonator system of Fig. 10, the frequency of each vibration mode corresponds to a distinct peak in the force-to-displacement frequency characteristic, and to a distinct, physical mode shape of the coupled mechanical resonator system. In the lowest frequency mode, all resonators vibrate in phase; in the middle frequency mode, the center resonator ideally remains motionless, while the end resonators vibrate 180^o out of phase; and finally, in the highest frequency mode, each resonator is phase-shifted 180^o from its adjacent neighbor. Without additional electronics, the complete mechanical filter exhibits the jagged passband seen in Fig. 11. As will be shown, termination resistors designed to lower the *Q*'s of the input and output resonators by specific amounts are required to flatten the passband and achieve a more recognizable filter characteristic, such as in Fig. 9.

In practical implementations, because planar IC processes typically exhibit substantially better *matching* tolerances than *absolute*, the constituent resonators in μmechanical filters are normally designed to be identical, with identical dimensions and resonance frequencies. For such designs, the center frequency of the overall filter is equal to the resonance frequency f_o of the resonators, while the filter passband (i.e., the bandwidth) is determined by the spacings between the mode peaks.

The relative placement of the vibration peaks in the frequency characteristic—and thus, the passband of the eventual filter—is determined primarily by the stiffnesses of the coupling springs (k_{sij}) and of the constituent resonators at the coupling locations (k_r). Specifically, for a filter with center frequency f_o and bandwidth B, these stiffnesses must satisfy the expression[19]

$$B = \left(\frac{f_o}{k_{ij}}\right)\left(\frac{k_{sij}}{k_r}\right) \tag{6}$$

where k_{ij} is a normalized coupling coefficient found in filter cookbooks.[20] Note from (6) that filter bandwidth is not dependent on the absolute values of resonator and coupling beam stiffness; rather, their ratio k_{sij}/k_r dictates bandwidth. Thus, the procedure for designing a mechanical filter involves two main steps: first, design of a mechanical resonator with resonance frequency f_o and adjustable stiffness k_r; and second, design of coupling springs with appropriate values of stiffness k_{sij} to enable a desired bandwidth within the adjustment range of resonator k_r's.

To take advantage of the maturity of *LC* ladder filter synthesis techniques, the enormous database governing *LC* ladder filter implementations,[20] and the wide availability of electrical circuit simulators, realization of the μmechanical filter of Fig. 10(a) often also involves the design of an *LC* ladder version to fit the desired specification. The elements in the *LC* ladder design are then matched to lumped mechanical equivalents via electromechanical analogy, where inductance, capacitance, and resistance in the electrical domain equate to mass, compliance, and damping, respectively, in the mechanical domain. Figure 10(b) explicitly depicts the equivalence between the filter's lumped mass-spring-damper circuit and its electrical equivalent circuit. As shown, for this particular electromechanical analogy (the current analogy), each constituent resonator corresponds to a series *LCR* tank, while each (massless) coupling spring ideally corresponds to a shunt capacitor, with the whole coupled network corresponding to an *LC* ladder bandpass filter.

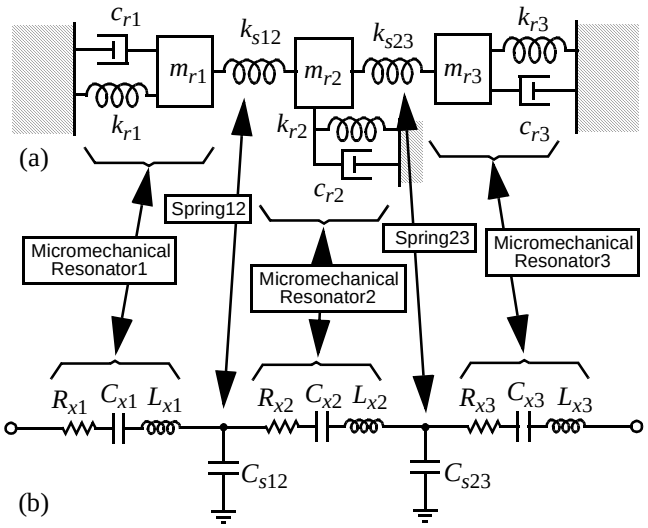

Fig. 10. (a) Equivalent lumped parameter mechanical circuit for a mechanical filter. (b) Corresponding equivalent *LCR* network.

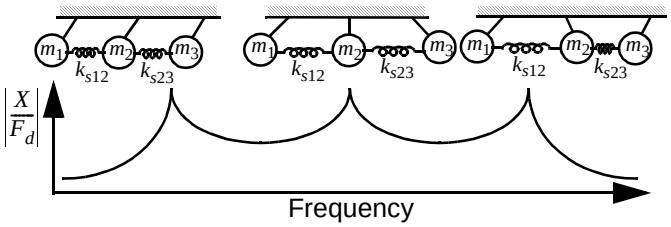

Fig. 11. Mode shapes of a three-resonator micromechanical filter and their corresponding frequency peaks.

4.2. A Two-Resonator, Tunable, Switchable, VHF Micromechanical Filter

Figure 12 shows the perspective-view schematic of a practical two-resonator micromechanical filter[9,11] capable of operation in the HF to VHF range. As shown, the filter consists of two μmechanical clamped-clamped beam resonators, coupled mechanically by a soft spring, all suspended 0.1 μm above the substrate. Conductive (polysilicon) strips underlie each resonator, the center ones serving as capacitive transducer electrodes positioned to induce resonator vibration in a direction perpendicular to the substrate, the flanking ones serving as tuning electrodes capable of voltage-controlled tuning of resonator frequencies. The resonator-to-electrode gaps are determined by the thickness of a sacrificial oxide spacer during fabrication and can thus be made quite small (e.g., 0.1 μm or less) to maximize electromechanical coupling.

Under normal operation, the device is excited capacitively by a signal voltage v_i applied to the input electrode through the termination resistor R_{Q1}, which controls the Q of the input resonator to achieve a flat passband. The output is taken at the other end of the structure, also via capacitive transduction. Upon application of an input v_i with suitable frequency, the constituent resonators begin to vibrate in one or more flexural modes in a direction perpendicular to the substrate. For a properly designed mechanical filter, if the excitation voltage has a frequency within the passband, both resonators will vibrate. Vibration of the output resonator then couples to the output electrode, providing an output current i_{x2} given by an equation similar to (5). The current i_{x2} is then directed to resistor R_{Q2}, which provides the proper termination impedance for the μmechanical filter and

converts i_{x2} to a proper output voltage v_o.

In effect, the operation of the above filter can be briefly summarized as follows:

(1) An electrical input signal is applied to the input port and converted to an input force by the electromechanical transducer (which for the case of Fig. 12(a) is capacitive) that can then induce mechanical vibration in the x direction;

(2) mechanical vibration comprises a mechanical signal that is processed in the mechanical domain—specifically, the signal is rejected if outside the passband of the filter, and passed if within the passband; and

(3) the mechanically processed signal appears as motion of the output resonator and is re-converted to electrical energy at the output transducer, ready for processing by subsequent transceiver stages.

4.2.1. VHF Filter Design

As can be surmised from Fig. 10(b), the network topologies for the mechanical filters of this work differ very little from those of their purely electronic counterparts, and in principal, can be designed at the system-level via a procedure derived from well-known, coupled resonator ladder filter synthesis techniques. In particular, given the equivalent *LCR* element values for a prototype μmechanical resonator, it is possible to synthesize a mechanical filter entirely in the electrical domain, converting to the mechanical domain only as the last step. However, although possible, such a procedure is not recommended, since knowledge and ease of design in both electrical and mechanical domains can greatly reduce the effort required.

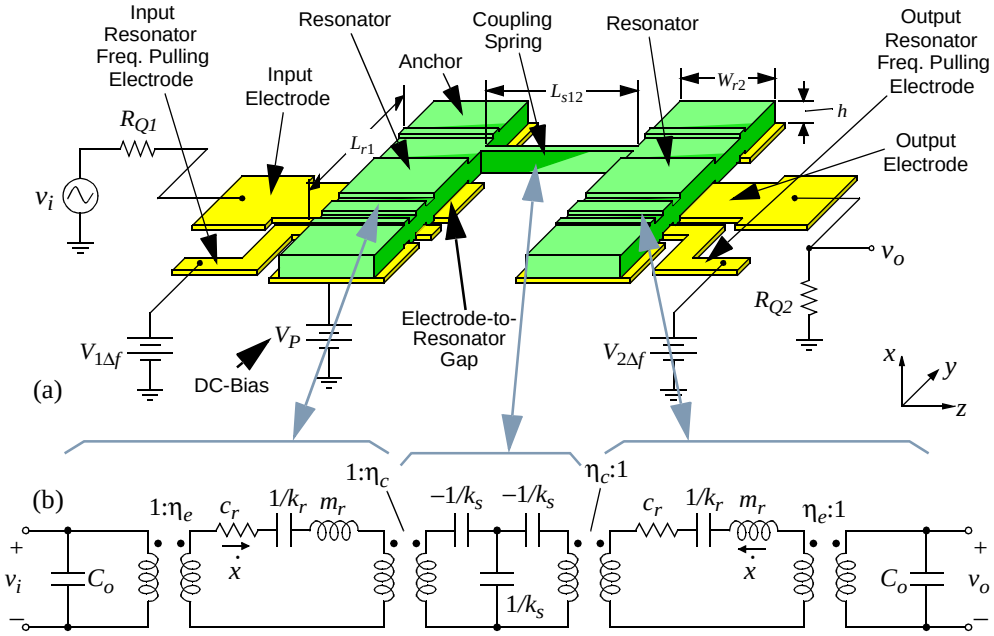

Fig. 12. (a) Perspective-view schematic of a two-resonator VHF μmechanical filter with typical bias, excitation, and signal conditioning electronics. (b) Electrical equivalent circuit for the filter in (a). Here, m_r, k_r, and c_r denote the mass, stiffness, and damping of the (identical) resonators at the drive electrode locations, and $\eta_e = V_P(\partial C/\partial x)$ and $\eta_c = (k_{rc}/k_r)^{0.5}$ are turns ratios modeling electromechanical coupling at the inputs and mechanical impedance transformations at low velocity coupling locations.

The design procedure for the two-resonator micromechanical filter of this work can be itemized as follows:

(1) *Design and establish the* μ*mechanical resonator prototype to be used, choosing necessary geometries for the needed frequency and insuring that enough electrode-to-resonator transducer coupling is provided to allow for predetermined termination resistor values.* With predetermined values of W_r, h, W_e, V_P, and R_Q, this amounts to solving for the resonator length L_r and electrode-to-resonator gap spacing d that simultaneously satisfy (2) and the equation for the needed termination resistor[10]:

$$R_{Qn} = \left(\frac{Q_{res}}{q_n Q_{fltr}} - 1\right)\frac{c_r}{\eta_e^2} = \left(\frac{Q_{res}}{q_n Q_{fltr}} - 1\right)R_{xn}\,, \tag{7}$$

where Q_{res} is the uncontrolled quality factor of the constituent resonators, $Q_{fltr} = f_o/B$, n refers to the port in question, q_n is a normalized q parameter obtained from a filter cookbook,[20] c_r and η_e are defined in the caption of Fig. 12(b), and R_x is the series motional resistance of an end resonator.

(2) *Choose a manufacturable value of coupling beam width* W_s *and design coupling beam(s) corresponding to a "quarter-wavelength" of the filter center frequency.* Here, the coupling beam is recognized as an acoustic transmission line that can be made transparent to the filter when designed with quarter-wavelength dimensions.[10,21] For a flexural-mode coupling beam, neglecting rotational movements at the resonator attachment points, quarter-wavelength dimensions are achieved

when W_s and L_s are chosen to satisfy the expression[9]

$$H_6 = \sinh\alpha\cos\alpha + \cosh\alpha\sin\alpha = 0\,, \tag{8}$$

where $\alpha=L_s(\rho W_s h\omega^2/(EI_s))^{0.25}$, $I_s=W_s h^3/12$, and needed dimensions are given in Fig. 12(a). Note that in choosing W_s and L_s to satisfy (8), the coupling beam stiffness k_{s12} is constrained to a particular value, given by[9]

$$k_{s12} = -\frac{EI_s\alpha^3(\sin\alpha + \sinh\alpha)}{L_s^3(\cos\alpha\cosh\alpha - 1)}\,. \tag{9}$$

Note that this also constrains the ability to set the bandwidth of the filter via the coupling beam dimensions, and thus, necessitates an alternative method for setting bandwidth.

(3) *Determine the coupling location(s) on the resonators corresponding to the filter bandwidth of interest.* This procedure is based upon two important properties of this filter and the resonators comprising it: First, the filter bandwidth B is determined not by absolute values of stiffness, but rather by a ratio of stiffnesses (k_{s12}/k_r); and second, the value of resonator stiffness k_r varies with location (in particular, with velocity) and so can be set to a desired value by simply choosing an appropriate coupling beam attachment point. Specifically, the resonator stiffness k_r can be expressed as[21]

$$k_r(y) = \omega_o{}^2 m_r(y)\,, \tag{10}$$

where ω_o is the radian resonance frequency, m_r is effective mass as a function of location given by

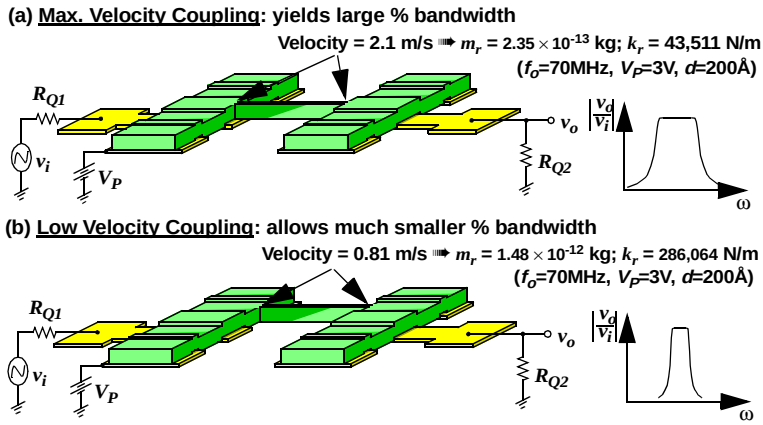

Fig. 13. Filter schematics showing (a) maximum velocity coupling to yield a large percent bandwidth and (b) low velocity coupling to yield a smaller percent bandwidth.

$$m_r(y) = \frac{\rho W_r h\int_0^{L_r}[X(y')]^2 dy'}{[X(y)]^2}\,, \text{ where } X(y) = (\cos ky - \cosh ky) - \sigma_n(\sin ky - \sinh ky)\,, \tag{11}$$

and where ρ is the density of the structural material, $k = 4.73/L_r$ and σ_n=0.9825 for the fundamental mode, and dimensions are indicated in Fig. 5 or 12(a). Figure 13 illustrates how the choice of coupling beam attachment point can greatly influence the bandwidth of a mechanical filter. In Fig. 13(a), the coupling beam is attached at the highest velocity point, where the resonator presents its smallest stiffness, resulting in a very wide filter bandwidth. On the other hand, Fig. 13(b) depicts coupling at a lower velocity point closer to the resonator anchors, where the resonator presents a much higher stiffness, leading to a much smaller percent bandwidth, as dictated by (6). In effect, the bandwidth of the filter is set not by choosing the coupling beam stiffness k_{s12}, but rather by choosing an appropriate value of resonator stiffness k_r to satisfy (6), given a k_{s12} constrained by quarter-wavelength design.

(4) *Generate a complete equivalent circuit for the overall filter and verify the design using a circuit simulator.* Figure 12(b) presents the equivalent circuit for a two-resonator micromechanical filter along with equations for the elements.

4.2.2. Tunability and Switchability

As can be seen from (2), through the electrical spring stiffness k_e, the resonance frequency of this device is tunable via adjustment of the dc-bias voltage V_P, and this can be used advantageously to implement filters with tunable center frequencies, or to correct for passband distortion caused by finite planar fabrication tolerances. This, combined with the switchability described in association with (3) and (5), makes the micromechanical filter of Fig. 12 nearly ideal for the RF channel-select architecture of Fig. 4. The switching nature of this device can actually be further exploited to implement a combined mixing and gain function in this same device. In particular, by introducing a local oscillator signal into the bias voltage of the input resonator, the square law voltage-to-force transfer function in the input transducer can be harnessed for both mixing and parametric gain. Using this principle, mixing, filtering, and gain in a single micromechanical device was recently demonstrated.[22]

4.3. VHF Micromechanical Filter Performance

The SEM for a 34.5 MHz, two-resonator, low-velocity coupled micromechanical filter constructed of phosphorous-doped polysilicon is shown in Fig. 14 along with relevant design dimensions. The measured transmission spectrum for an L_r/8-coupled version of this filter achieved with V_P=15V and R_{Qn}=2kΩ is presented in Fig. 15. As shown, a percent bandwidth of 1.3% was achieved with an associated insertion loss of less than 2 dB at its peak, and a stopband rejection exceeding 20 dB. With the use of additional resonators, even better performance is achievable, with sharper roll-offs (i.e., smaller shape factors) and larger stopband rejections.[10,11]

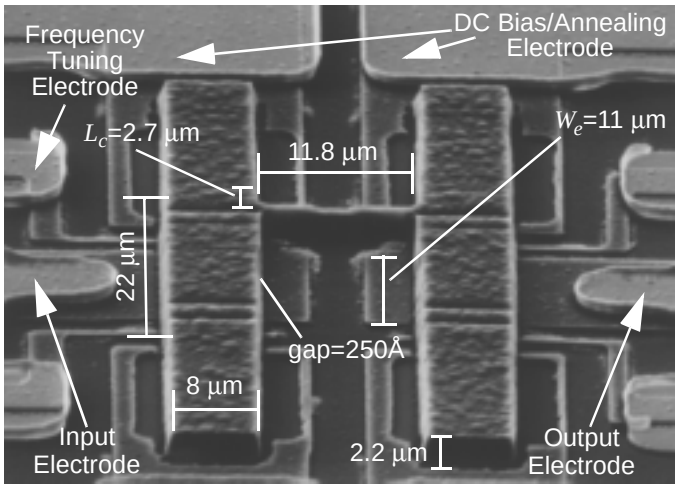

Fig. 14. SEM of a 34.5 MHz switchable, tunable, μmechanical filter with important dimensions.

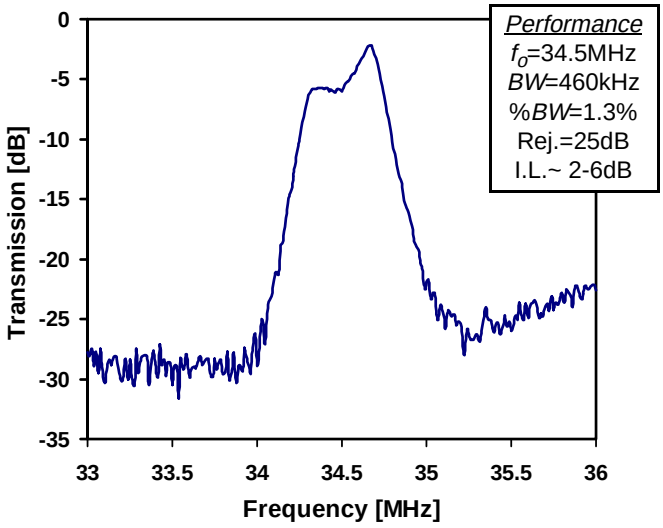

Fig. 15. Measured transmission spectrum for a VHF two-resonator micromechanical filter, such as shown in Fig. 14.

5. FREQUENCY RANGE OF APPLICABILITY

If micromechanical resonator devices are to realize the RF channel-select receiver architecture of Fig. 4 for military and commercial handset applications, then the low VHF frequency of Fig. 15 must be extended to the high VHF and UHF ranges. Thus, the ultimate frequency range of the described micromechanical resonators is of great interest and is presently a topic under intense study. From a purely geometric standpoint, the frequency range of micromechanical resonators can extend well into the gigaHertz range. For example, the dimensions of a clamped-clamped beam resonator required to attain a frequency of 1 GHz are (referring to Fig. 2) approximately L≈4 μm, W=2 μm, and h=2 μm, where finite-element analysis should be used to account for width and anchoring effects. This frequency can also be attained by longer beams vibrating in higher modes. Thus, according to analytical and finite element prediction, frequencies into the gigaHertz range are geometrically possible.

Geometry, however, is only one of many important considerations. The applicable frequency range of micromechanical resonators will also be a function of several other factors, including:

(1) quality factor, which may change with frequency for a given material, depending upon frequency-dependent energy loss mechanisms[23];

(2) series motional resistance R_x (c.f., Eq. (7)), which must be minimized to allow impedance matching with other transceiver components, to suppress input-referred noise, and to alleviate filter passband distortion due to parasitics[7,21];

(3) absolute and matching tolerances of resonance frequencies, which will both be functions of the fabrication technology and of frequency trimming or tuning strategies[24]; and

(4) stability of the resonance frequency against temperature variations, mass loading, aging, and other environmental phenomena.

Each of the above phenomena are currently under study. In particular, assuming adequate vacuum can be achieved, the ultimate quality factor will be strongly dependent upon the material type, and even the manufacturing process. For example, surface roughness or surface damage during fabrication may play a role in limiting quality factor. In fact, preliminary results comparing the quality factor achievable in diffusion-doped polysilicon structures (which exhibit substantial pitting of the poly surface) versus implant-doped ones, indicate that the latter exhibit almost an order of magnitude higher Q at frequencies near 10 MHz. The difference in Q is very intriguing, and is consistent with a surface roughness-dependent dissipation mechanism.

From a design perspective, one Q-limiting loss mechanism that becomes more important with increasing frequency is loss to the substrate through anchors. The frequency dependence of this mechanism arises because the stiffness of a given resonator

beam generally increases with resonance frequency, giving rise to larger forces exerted by the beam on its anchors during vibration. As a consequence, more energy per cycle is radiated into the substrate via the anchors, and Q degrades. Anti-symmetric resonance designs, such as balanced tuning forks, could prove effective in alleviating this source of energy loss.

Alternatively, anchor loss mechanisms can be greatly alleviated by using "anchor-less" resonator designs, such as shown in Fig. 16. This recently demonstrated device utilizes a free-free beam (i.e., xylophone) resonator suspended by four torsional supports attached at flexural node points.[25] By choosing support dimensions corresponding to a quarter-wavelength of the free-free beam's resonance frequency, the impedance presented to the beam by the supports can be effectively nulled out, leaving the beam virtually levitated and free to vibrate as if it had no supports.[25] Figure 17 presents the frequency characteristic for a 92.25 MHz version of this μmechanical resonator, showing a Q of nearly 8,000—still plenty for channel-select RF applications.

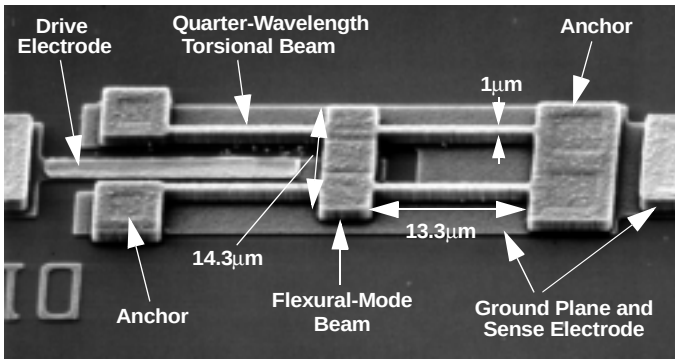

Fig. 16. SEM of free-free beam virtually levitated micromechanical resonator with relevant dimensions for f_o=71 MHz

A. Electromechanical Coupling.

In addition to possible Q limitations, the practical frequency range of micromechanical resonators is limited by electromechanical coupling, which is largest when the series motional resistance R_x is smallest. From (7), an expression for R_x can be written as

$$R_x = \frac{\sqrt{k_r m_r}}{Q V_P^2 (\partial C/\partial x)^2}, \qquad (12)$$

where k_r and m_r are the effective stiffness and mass of the resonator at the electrode location. Given that a frequency increase on this micro-scale entails an increase in k_r with only a slight decrease in mass m_r, (12) suggests that R_x increases gradually with frequency. For a given frequency, R_x may be reduced by increasing the dc-bias V_P or the $\partial C/\partial x$ term. The value to which V_P may be raised is limited by the available supply voltage, or by the maximum voltage obtainable through charge-pumping. The $\partial C/\partial x$ term is proportional to the electrode-to-resonator overlap area and is inversely proportional to the electrode-to-resonator gap spacing. The overlap area is limited by width effects on the resonance frequency, while the gap spacing is limited by technology. For the VHF filter described above, the gap spacing is defined by an oxide spacer thickness, and thus, can be made very small, on the order of tens to hundreds of Angstroms. For this reason, the minimum gap spacing is likely not determined by process limitations, but rather by dynamic range considerations.[21]

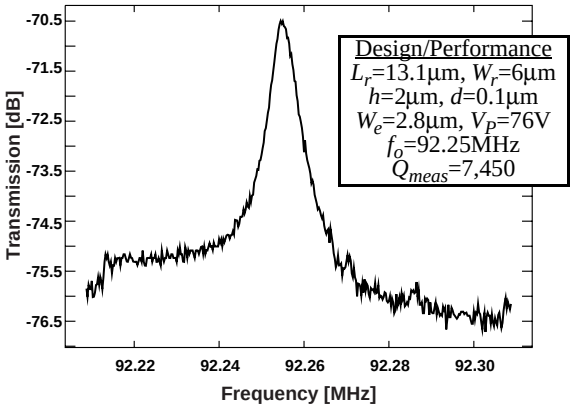

Fig. 17. Frequency characteristic for a fabricated 92.25 MHz free-free beam micromechanical resonator.

6. CONCLUSIONS

High-Q filters utilizing micromechanical vibrating resonator tanks have been demonstrated with frequencies from LF to VHF, and requiring areas of less than 0.005 mm^2 per device on average. The tiny size, high selectivity, switchability, and zero dc power consumption of these devices together may make possible transceiver architectures that can actually harness the selectivity (or Q) versus power trade-offs so often seen in communication subsystem design. In particular, when used in transceiver architectures that emphasize selectivity over complexity, such passive micromechanical signal processors can potentially enable substantial power savings by relaxing the power requirements of the surrounding transistor-based transceiver stages (e.g., LNA's, mixers, A/D converters).

From a purely geometrical standpoint, the described IC-compatible mechanical resonators should be able to achieve vibrational frequencies well into the gigaHertz range. However, considerations other than geometry, such as frequency-dependent loss mechanisms, electromechanical coupling, and matching tolerances, all of which affect the ultimate performance of the described filters, will most likely dictate the ultimate frequency range of this technology. For the case of filters, dynamic range and minimum detectable signal are found to be competing attributes in some designs.

7. ACKNOWLEDGMENTS

The author gratefully acknowledges substantial contributions from former and present graduate students, in particular Kun Wang, Ark-Chew Wong, and Frank Bannon III, who are responsible for the filter and resonator results. This work was supported under grants from the Defense Advanced Research Projects Agency (DARPA), the National Science Foundation (NSF), the Jet Propulsion Laboratory (NASA/JPL), and an Army Research Office (ARO) MURI.

8. REFERENCES

1. N. M. Nguyen and R. G. Meyer, "Si IC-compatible inductors and *LC* passive filters," *IEEE J. of Solid-State Circuits*, vol. SC-25, no. 4, pp. 1028-1031, Aug. 1990.
2. S. V. Krishnaswamy, J. Rosenbaum, S. Horwitz, C. Yale, and R. A. Moore, "Compact FBAR filters offer low-loss performance," *Microwaves & RF*, pp. 127-136, Sept. 1991.
3. A. A. Abidi, "Direct-conversion radio transceivers for digital communications," *IEEE J. Solid-State Circuits*, vol. 30, No. 12, pp. 1399-1410, Dec. 1995.
4. J. C. Rudell, *et al.*, "A 1.9-GHz Wide-Band IF Double Conversion CMOS Receiver for Cordless Telephone Applications," *IEEE J. of Solid-State Circuits*, vol. 32, no. 12, pp. 2071-2088, Dec. 1997.
5. C. T.-C. Nguyen, L. P.B. Katehi, and G. M. Rebeiz, "Micromachined devices for wireless communications (invited)," *Proc. IEEE*, vol. 86, no. 8, pp. 1756-1768, Aug. 1998.
6. W. C. Tang, T.-C. H. Nguyen, and R. T. Howe, "Laterally driven polysilicon resonant microstructures," *Sensors and Actuators*, **20**, 25-32, 1989.
7. C. T.-C. Nguyen and R. T. Howe, "An integrated CMOS micromechanical resonator high-*Q* oscillator," to be published in *IEEE J. of Solid-State Circuits*, April 1999.
8. C. T.-C. Nguyen and R. T. Howe, "Microresonator frequency control and stabilization using an integrated micro oven," *Digest of Technical Papers*, Transducers'93, Yokohama, Japan, pp. 1040-1043, June 7-10, 1993.
9. F. D. Bannon III and C. T.-C. Nguyen, "High frequency microelectromechanical IF filters," *Technical Digest*, 1996 IEEE Electron Devices Meeting, San Francisco, CA, Dec. 8-11, 1996, pp. 773-776.
10. K. Wang and C. T.-C. Nguyen, "High-order micromechanical electronic filters," *Proceedings*, 1997 IEEE International Micro Electro Mechanical Systems Workshop, Nagoya, Japan, Jan. 26-30, 1997, pp. 25-30.
11. K. Wang, *et al.*, "*Q*-enhancement of microelectromechanical filters via low-velocity spring coupling," *Proceedings*, IEEE International Ultrasonics Symposium, Toronto, Canada, Oct. 5-8, 1997, pp. 323-327.
12. T. A. Core, W. K. Tsang, S. J. Sherman, "Fabrication technology for an integrated surface-micromachined sensor," *Solid State Technology*, pp. 39-47, Oct. 1993.
13. R. D. Nasby, *et al.*, "Application of chemical-mechanical polishing to planarization of surface-micromachined devices," *Technical Digest*, 1996 Solid-State Sensor and Actuator Workshop, Hilton Head, SC, pp. 48-53, June 3-6, 1996.
14. J. M. Bustillo, G. K. Fedder, C. T.-C. Nguyen, and R. T. Howe, "Process technology for the modular integration of CMOS and polysilicon microstructures," *Microsystem Technologies*, **1** (1994), pp. 30-41.
15. B. E. Boser and R. T. Howe, "Surface micromachined accelerometers," *IEEE J. of Solid-State Circuits*, vol. 31, no. 3, pp. 366-375, March 1996.
16. N. Yazdi, *et al.*, "Micromachined inertial sensors," *Proc. IEEE*, vol. 86, no. 8, pp. 1640-1659, Aug. 1998.
17. Q. Meng, M. Mehregany, and R. L. Mullen, "Theoretical modelling of microfabricated beams with elastically restrained supports," *J. Microelectromech. Syst.*, vol. 2, no. 3, pp. 128-137, Sept. 1993.
18. W. E. Newell, "Miniaturization of tuning forks," *Science*, vol. 161, pp. 1320-1326, Sept. 1968.
19. R. A. Johnson, *Mechanical Filters in Electronics*, New York: John Wiley & Sons, 1983.
20. A. I. Zverev, *Handbook of Filter Synthesis*, New York: John Wiley & Sons, 1967.
21. C. T.-C. Nguyen, "Frequency-selective MEMS for miniaturized communication devices (invited)," *Proceedings, 1*998 IEEE Aerospace Conference, Snowmass, Colorado, March 21-28, 1998, pp. 445-460.
22. A.-C. Wong, H. Ding, and C. T.-C. Nguyen, "Micromechanical mixer+filters," *Technical Digest*, IEEE International Electron Devices Meeting, San Francisco, California, Dec. 6-9, 1998, pp. 471-474.
23. V. B. Braginskky, V. P. Mitrofanov, and V. I. Panov, *Systems With Small Dissipation*. Chicago: University of Chicago Press., 1985.
24. K. Wang, *et al.*, "Frequency-trimming and *Q*-factor enhancement of micromechanical resonators via localized filament annealing," *Digest of Technical Papers*, Transducers'97, Chicago, Illinois, June 16-19, 1997, pp. 109-112.
25. K. Wang, Y. Yu, A.-C. Wong, and C. T.-C. Nguyen, "VHF free-free beam high-*Q* micromechanical resonators," *Technical Digest*, 12th International IEEE Micro Electro Mechanical Systems Conference, Orlando, Florida, Jan. 17-21, 1999, pp. 453-458.